Tracking Deceased-Related Thinking with Neural Pattern Decoding of a Cortical-Basal Ganglia Circuit

Supplemental Information

Preprocessing of Stories and Pictures

Deceased and living control related stories were allowed to have different levels of valence and arousal because we sought to use stories that would provide the strongest representation of the characters. To control for the effects of valence and arousal the demographic control stories were designed to have equivalent valence and arousal as the deceased stories. This was done using a list of 13,915 English lemmas (base words) rated by over 2000 people for valence and arousal (1). The ratings for all nouns and verbs in the deceased-related stories were computed and a t-test was used to ensure that the overall valence and arousal averages for deceased-related and demographic control stories were not significantly different ($p>0.1$). When necessary, the demographic control stories were modified to be more similar to the deceased-related stories.

All images had a resolution of 72 pixels per inch, and were rescaled to have a height of 300 pixels. All pictures were gray-scaled, background-stripped, and normalized for intensity and luminance. All images were set to have the same average image intensity and luminance. Two of the three pictures provided by the subject were selected for use in the task.

Imaging

Blood-oxygen-level dependent (BOLD) images were acquired on a GE 3-T scanner parallel to the anterior commissure-posterior commissure (AC-PC) line with a T2*-weighted EPI sequence of 45 contiguous slices (TR=2000ms, TE=25ms, flip angle = 77, FoV=192 x 192mm) of 3mm thickness and 3x3 in-plane resolution. Structural images were acquired with a T1-weighted

SPGR sequence recording 256 slices at a slice thickness of 1mm and in-plane resolution of 1x1mm.

Preprocessing was carried out using FSL version 6 (FMRIB's Software Library, www.fmrib.ox.ac.uk/fsl) (2). Preprocessing included slice time correction, motion correction, skull stripping and smoothing with a Gaussian kernel of 6mm FWHM. A 120-second high pass filter was applied to the data. All data were corrected for head motion by removing the influence of six motion time courses. Bias field correction was implemented using FSL-FAST for functional and structural images (3). Following preprocessing functional images were registered to structural images with 7-degrees of freedom and then structural images were warped to the standard MNI space using a 12-degree affine registration followed by a non-linear warp implemented in FNIRT (4, 5).

Least Squares Deconvolution

Our use of five second blocks followed by a 10 second nuisance regressor immediately afterwards required the deconvolution of BOLD data for use as input in a multivariate model. We therefore applied a least squares deconvolution method (Least Squares – Separate; LS-S) as described in (6) implemented in FSL 6.0 (FMRIB, /fsl.fmrib.ox.ac.uk/)(2). In this method parameter estimates for each individual trial are calculated and then analyses are conducted on the parameter estimates rather than raw BOLD signal. This method is suitable for multivariate analyses because it absolves the need to incorporate the hemodynamic response function in the multivariate model. Parameter estimates for each trial were calculated by creating a single trial regressor and all other trials as well as standard six-degree motion regressors were included as covariates. All regressors were convolved with a double gamma hemodynamic response function. Parameter estimates were then standardized for each run using the average and standard deviation of all parameter estimates for a given run within a given subject. Parameter estimates were warped to standard MNI space using FNIRT. Standardization and all

following analyses were implemented in MATLAB (MATLAB and Statistics Toolbox Release 2016, The MathWorks, Inc., Natick, Massachusetts, United States).

Rationale for Using T-Tests

The univariate analyses in this study were designed for feature selection for the multivariate analysis. For this reason, preprocessing and analytic steps were guided by the principle of maintaining similarity with the multivariate analysis. This would ensure that the characteristics of the univariate feature selection (i.e. deceased >control) would translate best into the multivariate analysis. As a result, univariate analyses were performed using T-tests rather than the hierarchical mixed effects model employed by standard neuroimaging packages such as FSL. A hierarchical model creating subject level means would diverge significantly from the multivariate analysis, which uses individual runs as inputs.

Model Training

We used l_2-norm regularized linear logistic regression to maximally separate the projected BOLD signal of deceased trials (D_PIC and D_STO) on one hand, and control trials (CLD_PIC and CLD_STO) on the other hand. The number of deceased trials was 351 and the number of control trials was 698. L_2-norm regularized linear logistic regression optimizes the cost function $\sum_{i=1}^{N}[y_i \boldsymbol{x}_i \boldsymbol{\beta} - N\log(1 + e^{\boldsymbol{x}_i \boldsymbol{\beta}})] + \lambda \sum_{j=1}^{K} \beta_j$, where N is the number of trials, K is the number of voxels in the mask, y_i is the class label of the i-th trial, encoded as +1 for deceased trials, and as -1 for control trials, $\boldsymbol{x}_i$ is the vector of BOLD data for the i-th trial, and $\boldsymbol{\beta} = [\beta_1, \ldots, \beta_K]^T$ are linear regression coefficients mapping BOLD data to class labels. The constant λ implements a tradeoff between model fidelity and model complexity as measured by the sum of squared regression coefficients. λ was optimized using 10x10 fold cross validation in order to maximize the model's prediction accuracy on hold out data. That is, the blocks were randomly split into 10

parts (folds), where nine folds were used to train the models (one for each choice of the regularization constant), and the tenth fold was used to measure the out-of-sample classification accuracy of the model in terms of the area under the receiver operating curve (AUC). Each fold served as holdout set once, and the procedure was repeated ten times for different random splits of the data, giving rise to 100 out-of-sample AUC scores per regularization constant. AUC values were averaged to yield one value per choice of the regularization constant. The entire analysis was repeated for 100 randomly permuted vectors of class labels, which allowed us to test the statistical significance of the obtained classifications against a null distribution. The optimal regularization constant was chosen as the maximizer of this value, and used to train a final model based on the data of all trials.

Null MVPA Analyses

We sought to highlight the specificity of the model training using the conjunction results. To do this, two null regions were selected and both an MVPA model and prediction of deceased-related thinking were computed with these regions. The null regions were selected by identifying two 8mm-spheres with no voxels associated with pictures, stories or thinking about the deceased. One sphere was located in the left post central gyrus (Sphere Center= 60, 46, 66) and another sphere was identified on the midline in the lingual gyrus (Sphere Center= 46, 22, 34). Each sphere comprised 257 voxels in order to approximate the conjunction mask, which was 243 voxels.

To assess the significance of MVPA discrimination we identified a null distribution by permuting the labels of deceased *vs*. control blocks and determined the degree that the MVPA model predicted the true labels as compared to permuted labels. For the conjunction mask the identification of condition type (deceased vs. control) across a range of lambdas was significantly greater for the true labels as compared to randomly permuted labels ($p<0.01$). By contrast, for both null regions the identification of condition type for true labels was no greater

than the identification of condition type for the randomly permuted labels ($p<0.2$) (Supplemental Figure S2).

To further highlight the specificity of our model training we computed the prediction of deceased-related thinking during the SART using the output from the null models. Both were insignificant (Null1: $B_{203}=2.11$, SE=1.8, p=0.24, Null2: $B_{203}=1.31$, SE=1.32, p=0.32).

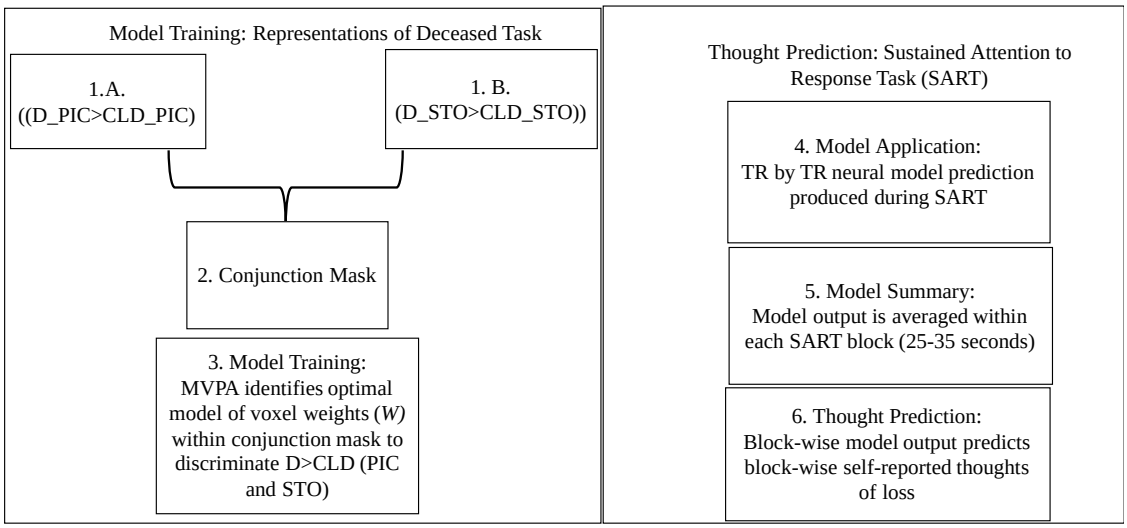

Supplemental Figure S1. Workflow of Present Study: This study incorporated 6 analytic steps. In the first steps (1 and 2) voxels were selected based on conjoint activation for both deceased pictures and deceased-related stories. These voxels were input into a machine learning analysis (3) that produced a model identifying the pattern of activity that optimally predicted condition type (Deceased or Control) during the picture and story blocks. This model was then applied to the SART data (4) and used to generate a TR-by-TR prediction of mental representations of the deceased occurring during the latter task. The average model prediction per block was computed (5) and used to predict deceased-related thinking in a given block (6).

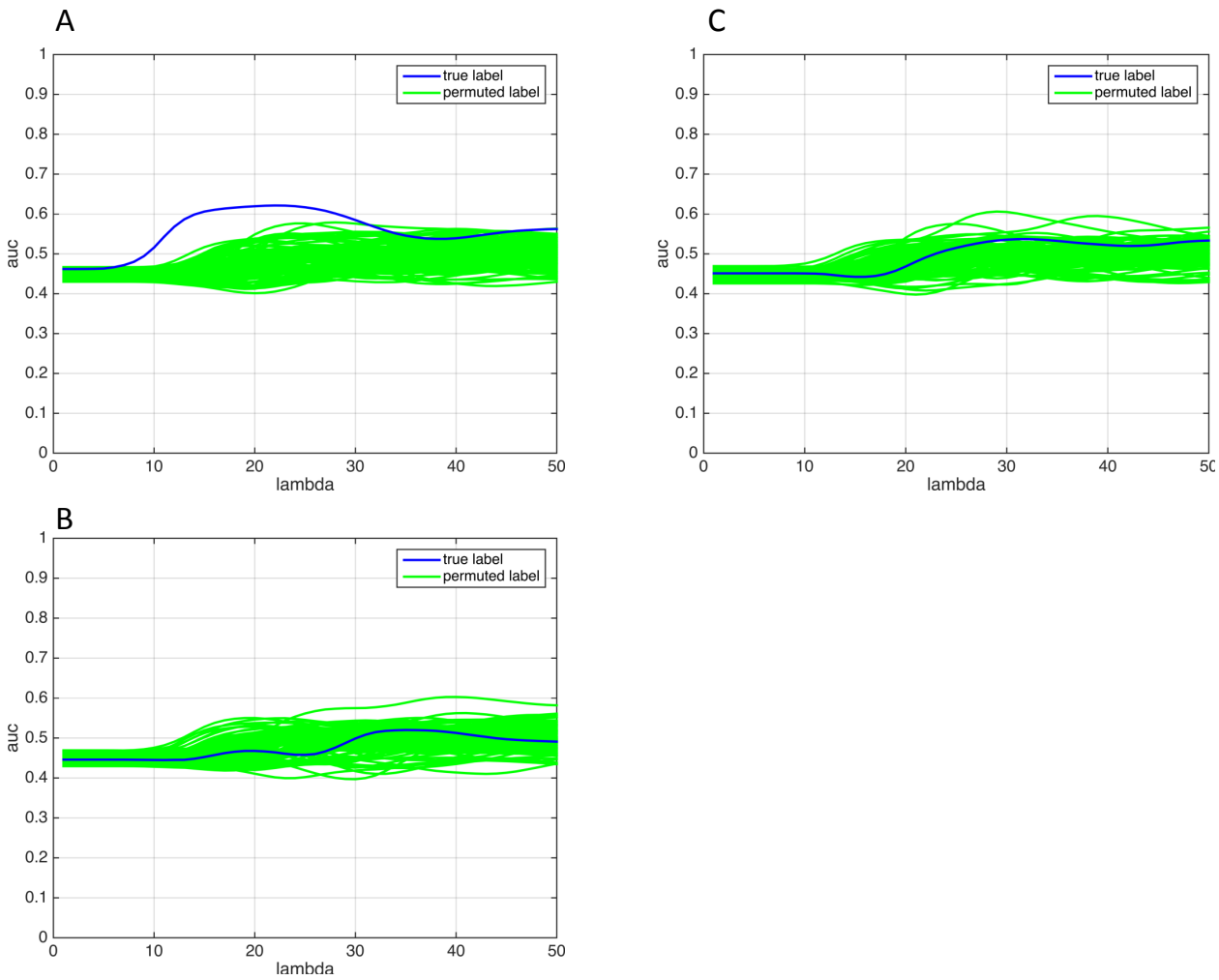

Supplemental Figure S2. MVPA discrimination. A. Performance of MVPA classifier predicting deceased *vs.* control blocks as compared to randomly permuted labels from a model trained in the conjunction mask. Across a range of lambdas there is significant prediction of block type for true labels but not permuted labels. **B and C.** Performance of MVPA classifiers trained in null regions of left post central gyrus and midline angular gyrus. No difference in prediction of true labels as compared to permuted labels is seen.

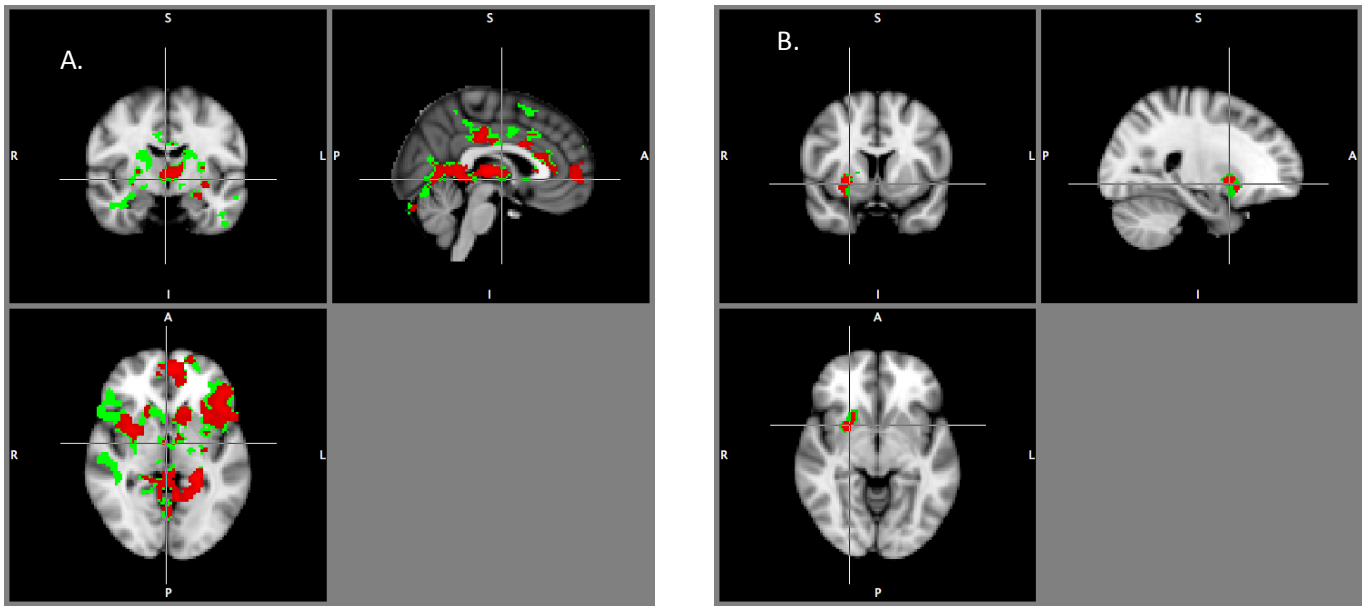

Supplemental Figure S3. Effects of Controlling for Arousal and Valence. A. Green mask displays clusters associated with stories of deceased versus control conditions when not accounting for valence/arousal. Red mask displays significant clusters when controlling for valence/arousal. Activity in bilateral hippocampus, superior temporal gyrus and left superior frontal gyrus is seen in green but not red mask. **B.** Effect of valence/arousal for picture contrast. A larger extent of voxels is seen in green but not red mask.

Table S1. Clusters activated by deceased-related stories as compared to control stories. Regions Activated by Stories of the Deceased: Regions across which clusters showing greater response to deceased-related as compared to control stories (D_STO>CLD_STO) were identified.

Region	#Voxels	X	Y	Z
Angular Gyrus	164	17.05	34.76	52.55
Central Opercular Cortex	29	40.07	66.69	37.45
Anterior Cingulate	577	43.58	74.25	47.26
Posterior Cingulate	1126	44.00	43.93	45.51
Frontal Medial Cortex	62	41.40	88.66	31.77
Frontal Operculum Cortex	295	24.41	72.19	37.50
Frontal Orbital Cortex	868	34.13	74.77	29.27
Frontal Pole	782	35.94	88.93	38.42
Inferior Frontal Gyrus	669	19.82	73.66	38.44
Inferior Temporal Gyrus	63	22.73	61.08	18.29
Insular Cortex	730	40.46	68.31	35.04
Intracalcarine Cortex	139	43.64	29.24	41.01
Lateral Occipital Cortex	161	17.32	30.25	48.94
Left Amygdala	69	32.55	60.58	28.04
Left Caudate	125	38.60	69.14	37.81
Left Hippocampus	152	33.39	46.76	32.75
Left Putamen	159	32.69	64.76	35.68
Left Thalamus	344	42.33	54.90	38.19
Lingual Gyrus	551	42.66	35.15	35.55
Middle Frontal Gyrus	231	30.17	76.45	55.30
Occipital Fusiform Gyrus	46	49.22	21.91	22.85
Paracingulate Gyrus	834	42.19	83.61	44.48
Parahippocampal Gyrus	269	34.31	48.08	29.42
Precentral Gyrus	21	15.86	66.95	40.57
Precuneous Cortex	875	43.87	34.95	43.34
Right Amygdala	37	58.57	62.78	28.38
Right Caudate	60	51.93	73.22	36.95
Right Hippocampus	32	55.03	44.25	37.09
Right Pallidum	12	56.58	60.08	36.58
Right Putamen	262	57.92	64.79	35.08
Right Thalamus	197	47.76	54.57	37.93
Subcallosal Cortex	14	41.64	72.29	34.36
Superior Frontal Gyrus	343	37.86	79.03	57.64
Supracalcarine Cortex	38	41.13	30.79	43.58
Supramarginal Gyrus	221	15.89	39.51	52.88

Region	#Voxels	X	Y	Z
Temporal Fusiform Cortex	12	29.67	45.75	27.50
Temporal Pole	248	33.94	70.23	24.77

Clusters are significant at a voxel-wise threshold of t_{523}=3.1, p<0.001 and cluster corrected with a threshold of p<0.05.

Table S2. Clusters activated by deceased-related pictures as compared to control pictures. Regions Activated by Pictures of the Deceased: Regions across which clusters showing greater response to deceased-related as compared to control pictures (D_PIC>CLD_PIC) were identified.

Region	#Voxels	X	Y	Z
Right Frontal Orbital Cortex	19	152	58.89	67.89
Right Insula	28	224	60.64	69.25
Right Caudate	16	128	52.69	73.06
Right Putamen	109	872	56.95	68.13

Clusters are significant at a voxel-wise threshold of t_{522}=3.1, p<0.001, cluster-p <0.05.

Supplemental References

1. Warriner AB, Kuperman V, Brysbaert M (2013): Norms of valence, arousal, and dominance for 13,915 English lemmas. *Behav Res Methods*. 45:1191-1207.
2. Woolrich MW, Jbabdi S, Patenaude B, Chappell M, Makni S, Behrens T, et al. (2009): Bayesian analysis of neuroimaging data in FSL. *Neuroimage*. 45:S173-186.
3. Zhang Y, Brady M, Smith S (2001): Segmentation of brain MR images through a hidden Markov random field model and the expectation-maximization algorithm. *IEEE transactions on medical imaging*. 20:45-57.
4. Jenkinson M, Bannister P, Brady M, Smith S (2002): Improved optimization for the robust and accurate linear registration and motion correction of brain images. *Neuroimage*. 17:825-841.
5. J.L.R. Andersson MJaSMS (2007): Non-linear registration, aka Spatial normalisation. *FMRIB technical report TR07JA2*.
6. Mumford JA, Turner BO, Ashby FG, Poldrack RA (2012): Deconvolving BOLD activation in event-related designs for multivoxel pattern classification analyses. *Neuroimage*. 59:2636-2643.